Chapter 1

Applications of Density Functional Theory in Soft Condensed Matter

Hartmut Löwen

Heinrich-Heine University Düsseldorf, Germany

Applications of classical density functional theory (DFT) to soft matter systems like colloids, liquid crystals and polymer solutions are discussed with a focus on the freezing transition and on nonequilibrium Brownian dynamics.

First, after a brief reminder of equilibrium density functional theory, DFT is applied to the freezing transition of liquids into crystalline lattices. In particular, spherical particles with radially symmetric pair potentials will be treated (like hard spheres, the classical one-component plasma or Gaussian-core particles).

Second, the DFT will be generalized towards Brownian dynamics in order to tackle nonequilibrium problems. After a general introduction to Brownian dynamics using the complementary Smoluchowski and Langevin pictures appropriate for the dynamics of colloidal suspensions, the dynamical density functional theory (DDFT) will be derived from the Smoluchowski equation. This will be done first for spherical particles (e.g. hard spheres or Gaussian-cores) without hydrodynamic interactions. Then we show how to incorporate hydrodynamic interactions between the colloidal particles into the DDFT framework and compare to Brownian dynamics computer simulations.

Third orientational degrees of freedom (rod-like particles) will be considered as well. In the latter case, the stability of intermediate liquid crystalline phases (isotropic, nematic, smectic-A, plastic crystals etc) can be predicted. Finally, the corresponding dynamical extension of density functional theory towards orientational degrees of freedom is proposed and the collective behaviour of "active" (self-propelled) Brownian particles is briefly discussed.

Contents

Introduction

Apart from their fundamental importance, soft matter materials (as colloidal dispersions, liquid crystals and polymer coils) represent excellent realizations of strongly interacting classical many-body systems. In this sense, soft matter provides us with *model systems* which in turn means that a reasonable (coarse-grained) modelling of soft matter is very realistic and can lead to valuable physical insight. This is one of the main reasons why theory, computer simulations and experiments go hand-in-hand in recent soft matter research.

A classical many-body system is typically characterized by "effective" pairwise interaction forces [1], derived from an (optimal) effective pair potential $V(r)$ where r denotes the interparticle distance [2]. Lots of theoretical and simulational efforts have been spent in the past to derive or to compute the effective interaction. Subsequently, once the effective pair interaction is known, equilibrium properties like structural correlations and phase transitions can be obtained by theory and computer simulation. This route can also be inversed: If for a particular shape of $V(r)$ novel behaviour is predicted by theory or computer simulation, various soft matter systems

(in particular mixtures) can be exploited to find a convenient realization of the prescribed potential $V(r)$.

While the concept of effective interactions is valid for static equilibrium quantities, it typically breaks down for dynamical correlations [3] and nonequilibrium situations [4]. The dynamics of colloidal particles and polymers in solution is Brownian due to the separation of time scales between the mesoscopic particles and the solvent molecules. The overdamped particle motion can be described using the Smoluchowski equation or the stochastically equivalent Langevin picture [5, 6]. A wealth of nonequilibrium effects have been discovered in these Brownian systems [7, 8].

In this book chapter we highlight the role of density functional theory in order to calculate phase diagrams in equilibrium and Brownian dynamics in nonequilibrium. Density functional theory represents a microscopic approach to many-body effects where the pair interaction potential $V(r)$ is the only input. Computer simulations, on the other hand, are necessary to provide "benchmark" data to test the theory. For the topics considered here, these are mainly Monte-Carlo simulations for the equilibrium phase diagrams and Brownian dynamics simulations for nonequilibrium dynamics. In this contribution, we focus in particular on the freezing transition of simple systems, governed by a radially-symmetric pair potential (e.g. hard or soft spheres) and on orientational degrees of freedom relevant for e.g. rodlike systems. For both cases, phase diagrams and effects of nonequilibrium Brownian dynamics are described. Some examples from recent research in this field are used to illustrate the capacity of dynamical density functional theory as compared to Brownian dynamics computer simulations [9].

1. Freezing of spheres

1.1. *Phenomenological results*

Experiments show that liquids freeze into periodic crystalline structures at low temperatures or high densities. In these states, the translational symmetry of the system is broken, i.e. the one-particle density

$$\rho(\vec{r}) = \left\langle \sum_{i=1}^{N} \delta(\vec{r} - \vec{r}_i) \right\rangle \tag{1.1}$$

is *inhomogeneous*. Here $\langle \dots \rangle$ denotes a canonical average, and $\vec{r}_i$ ($i = 1, \dots, N$) are the particle positions. As freezing is ubiquitous and general, it is one of the most important phase transition in nature. The basic ques-

tion is: when does it happen? Answering this question is one of the central tasks of statistical physics. A full microscopic theory is highly desirable which uses the interaction forces as an input and predicts the thermodynamic conditions for freezing as an output. Since freezing is a collective effect, this is a very demanding task.

Before turning to such a microscopic approach, let us first collect some *empirical facts* for freezing, as for more details and references, see [10–15]. We shall also summarize known phase behaviour for simple model potentials gained by computer simulations.

i) Lindemann-criterion of melting

If $a = \rho^{-1/3}$ denotes a typical interparticle spacing (with the number density ρ being the number of particles per volume), then one can examine the root mean-square displacement u of a particle around a given crystalline lattice position $\vec{R}_i$, i denoting a lattice site index, which is defined as

$$u = \sqrt{\langle (\vec{r_i} - \vec{R}_i)^2 \rangle} \tag{1.2}$$

This quantity can also be viewed as the spread of the inhomogeneous one-particle density $\rho(\vec{r})$ around a lattice position, see Figure 1.1.

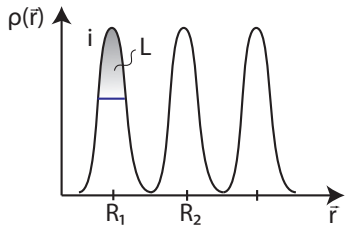

Fig. 1.1. One-dimensional sketch of the inhomogeneous one-particle density $\rho(\vec{r})$ in a crystalline solid with lattice points at $\vec{R}_1$ and $\vec{R}_2$. The spread of the density peak is embodied in the Lindemann parameter L.

The Lindemann parameter $L = u/a$ measures the fluctuations around the lattice positions in terms of the lattice constant. The traditional Lindemann rule of melting states that a solid melts if $L \approx 0.1$. Computer simulations have confirmed this phenomenolgical rule where the actual value of L at melting varies between 0.129 for hard spheres and 0.18 for the one-component plasma. But it is always roughly one order of magnitude smaller

than the lattice constant itself.

ii) Hansen-Verlet rule of freezing

Different to the Lindemann rule, the Hansen-Verlet rule starts from the liquid side of the freezing transition and states that the freezing occurs if the amplitude of the first peak in the liquid structure factor $S(k)$ exceeds 2.85. Originally found for Lennard-Jones systems, this rule has been confirmed also for other interactions like hard-sphere, plasma and Yukawa pair potentials. Without any notable exception a value of 2.5-3.0 was found near equilibrium freezing. However, the peak can be much higher in a metastable glassy state.

1.2. *Independent treatment of the different phases*

The simplest theoretical approach is to construct different theories for the different thermodynamic states (solid and liquid). In particular the internal energy of the solid phase can be accessed by a simple lattice sum of the given pair potentials. In particular, different candidate lattices can be assumed at fixed averaged density, and the one with minimal potential energy will be the stable one for temperature $T = 0$. Finite temperature corrections based on a harmonic phonon-picture can be added on top of that resulting in a (Helmholtz) free energy F of the solid state.

Likewise the free energy of the liquid can be gained by using for instance liquid integral equation theories [16] where different closure schemes may be adopted. Combined with the free energy of the solid, a Mawell double-tangent construction for the isothermal free energy per particles versus density ρ leads to the coexisting liquid and solid densities ρ_ℓ and ρ_s, see Figure 1.2. The double tangent ensures the equality of the chemical potential and the pressure in the two phases. If this is repeated for various temperature, the full phase diagram emerges. In three spatial dimensions, freezing is typically a first order transition with a considerable density jump $\Delta\rho = \rho_s - \rho_\ell$.

1.3. *Unifying Microscopic theories*

Both from a fundamental and esthetic point of view, a unifying theory which treats both the liquid and the solid phase on the same footing is desirable.

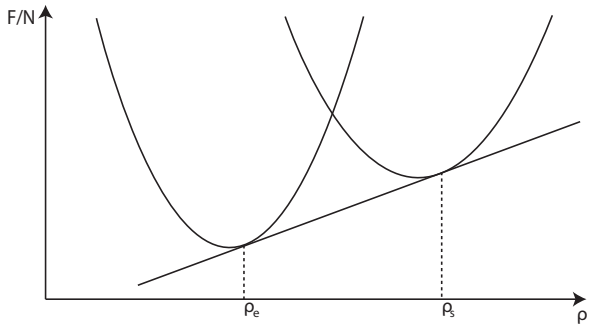

Fig. 1.2. Sketch of the Maxwell double tangent construction to the free energy per particle in the liquid and solid phase resulting in the two coexistence densities ρ_ℓ and ρ_s.

In the past decades, there have been considerable advances in this field. In three spatial dimensions, classical density functional theory (DFT) can be used to get a liquid-based description of the solid phase. Here the solid is viewed as a strongly inhomogeneous liquid with strong density peaks. Freezing in DFT is therefore a condensation of liquid density modes [14].

Conversely, in two spatial dimensions the Kosterlitz-Thouless approach is a solid-based approach which treats the liquid as a solid phase with an accumulation of defects.

In the following we shall focus on the three-dimensional freezing and on density functional theory. We emphasize that a unifying treatment is mandatory for the description of solid-liquid interface and phenomena like crystal nucleation and growth out of an undercooled melt where indeed a single theory for both phases is needed.

1.4. *Phase diagrams of simple potentials*

Let us first summarize some familiar phase diagrams for various model pairwise interactions. These were obtained mainly by "exact" computer simulation of a many-body system [17] and therefore provide "benchmark" data for a microscopic theory.

a) **Hard spheres**

The simplest nontrivial interaction potential is that for hard spheres of diameter σ . The potential reads

$$V(r) = \begin{cases} \infty, & r \leq \sigma \\ 0, & r > \sigma \end{cases} \tag{1.3}$$

The internal energy is completely ideal $U = \frac{3}{2}Nk_BT$, i.e. the averaged potential energy is zero. Hence Helmholtz free energy $F = U - TS$ scales with k_BT alone (as k_BT is the only energy scale for hard spheres). Therefore, for hard spheres, the entire thermodynamic behaviour is governed by entropy alone. This becomes different for other interactions which possess an explicit energy scale. This is the main reason why hard spheres are the most important models for freezing. From computer simulations, the hard sphere phase diagram is shown in Figure 1.3. The only parameter is the density which is conveniently scaled in terms of a volume or packing fraction $\eta = \pi\rho\sigma^3/6$. The quantity η measures the ratio of the volume occupied by all spheres to the total available volume V of the system. For $\eta \to 0$ an ideal gas is recovered, while maximal packing fo hard spheres occurs for $\eta = \eta_{cp} = 0.74$ corresponding to stacked layers of triangular crystals. In between, there is a first order freezing transition with coexisting packing fractions $\eta_{ell} = 0.494$ and $\eta_s = 0,545$. The stable crystalline crystal is face-centred-cubic (fcc) which has an ABC stacking sequence. Interestingly, the freezing transition is driven by entropy. For $\eta > \eta_s$ the solid state has a higher entropy than the fluid state clearly showing that entropy has nothing to do with structural order. More intuitively, a disordered fluid state at high densities implies jammed configurations, and much more configuration (i.e. higher entropy) is gained by taking as a reference configuration a solid and generating more configurations from slightly displaced particles (configurational entropy).

b) **Plasma**

The one-component plasma (OCP) with neutralizing background is defined by the pairwise Coulomb potential $V(r) = V_0/r$. By scaling the classical partition function, one can show that only the coupling parameter $\Gamma = \frac{\sqrt[3]{\frac{4\pi\rho}{3}}V_0}{k_BT}$ determines the structure and phase behaviour. There is isochoric freezing from the fluid into a body-centered-crystal (bcc) at $\Gamma = 178$.

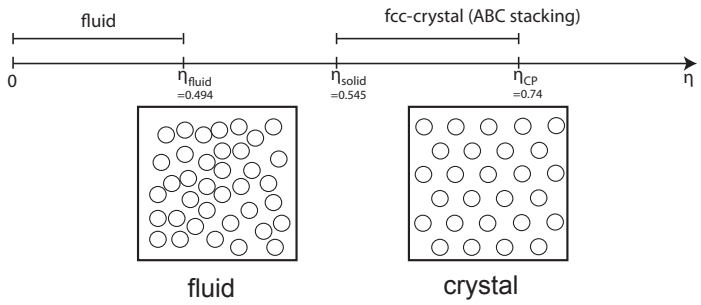

Fig. 1.3. Hard sphere freezing diagram versus packing fraction η. The intuitive picture of freezing is also shown: at high densities a fluid state involves blocked configurations and more configurations are achieved by a periodic packing.

c) **Soft spheres**

Inverse power law potentials where $V(r) = V_0(\sigma/r)^n$ interpolate between the plasma ($n = 1$) and the hard sphere potential, formally obtained as $n \to \infty$. Depending on n either bcc or fcc crystals are stable.

d) **Yukawa-system**

The Yukawa potential $V(r) = V_0 \exp(-\kappa r)/r$ applies e.g. to charge-stabilized colloidal suspensions. Again κ interpolates between the OCP ($\kappa = 0$) and the hard-sphere-limit $\kappa \to \infty$. The phase diagram depends only on $\lambda = \kappa a$ ($a = \rho^{-\frac{1}{3}}$) and $\tilde{T} = \frac{k_B T}{V_0} \frac{e^\lambda}{\lambda}$ and involves a fluid, a bcc solid and an fcc solid with a triple point as sketched in Figure 1.4.

e) **Lennard-Jones-system**

The Lennard-Jones potential, the traditional model for rare gases, is given by $V(r) = 4\epsilon \left(\left(\frac{\sigma}{r}\right)^{12} - \left(\frac{\sigma}{r}\right)^{6} \right)$ where ϵ is the energy and σ is the length scale. This potential has a long-ranged attractive tail. Correspondingly it exhibits also a critical point separating a gas from a liquid and a triple point with gas-liquid-fcc solid coexistence.

f) **Sticky hard spheres**

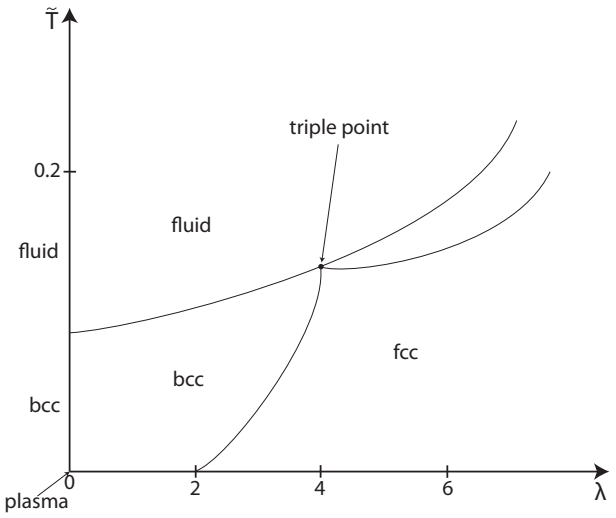

Fig. 1.4. Sketch of the Yukawa phase diagram in the plane spanned by λ and $\tilde{T}$. The special case $\lambda = 0$ is the one-component plasma.

Sticky hard sphere possess a square-well attraction and are reasonable models for proteins. Here

$$V(r) = \begin{cases} \infty & r \leq \sigma \\ -\epsilon & \sigma \leq r \leq \sigma(1+\delta) \\ 0 & \text{elsewhere} \end{cases} \tag{1.4}$$

with a finite attraction range $\delta\sigma$ and an attraction depth of $-\epsilon$. The scaled range δ must be larger than about 0.25 in order to get a liquid-gas separation. For small $\delta < 0.05$ there is a novel isostructural solid-solid-transition with a critical point [18].

g) **Ultrasoft interactions**

Soft (floppy) objects like polymer coils have effective interactions which are even softer than the plasma, therefore these interactions are called "ultrasoft" [19]. A log-Yukawa interaction has been proposed for star polymers. Here the interaction diverges at the origin only logarithmically with distance, i.e. $V(r) \propto k_B T \ln(r/\sigma)$. The phase behaviour [20] involves fluid,

bcc and fcc solids as well as body-centered-orthogonal and diamond lattices and exhibits reentrance effects.

h) **Penetrable interactions**

One may even describe soft objects with pair potentials which are finite at the origin. Examples are Gaussian potentials which are a good model for linear polymer coils. The phase behaviour involves again the fluid, bcc-solid and fcc-solid phase with fluid reentrance [21]. Penetrable interactions with other shapes exhibit again also "exotic" solid phases and reentrance [22]. Finite potentials which have a negative Fourier transform exhibit cluster crystals [23] where a lattice points is occupied by more than one particle.

To summarize:

(1) Hard and "harsh" potentials freeze into fcc lattices.
(2) Soft repulsive potentials with an at least $\frac{1}{r}$ singularity for $r \searrow 0$ freeze into bcc lattices.
(3) Ultrasoft $v(r) \sim -ln(\frac{r}{\sigma})$ and penetrable ($V(r \searrow 0) = V(0) < \infty$) potentials show besides fcc and bcc structures, more open "exotic" lattices and reentrance effects.
(4) If the Fourier transform of $V(r)$ has negative parts, a cluster crystal occurs.
(5) Attractions lead to gas-liquid coexistence and isostructural solid-solid transition.

In conclusion, various shapes of the pairwise interaction potential can lead to a rich phase behaviour and there is the theoretical challenge to construct a microscopic approach in order to predict and reproduce this complex phase behaviour. As will be discussed in the sequel, classical density functional theory for inhomogneous fluids does provide such an approach.

1.5. *Density Functional Theory (DFT)*

a) Basics

The cornerstone of density functional theory (DFT) is an existence theorem combined with a basic variational principle [10]. In detail, there exists a unique grand-canonical free energy-density-functional $\Omega(T, \mu, [\rho])$, which

gets minimal for the equilibrium density $\rho_0(\vec{r})$ and then coincides with the real grandcanoncial free energy, i.e.

$$\left.\frac{\delta\Omega(T,\mu,[\rho])}{\delta\rho(\vec{r})}\right|_{\rho(\vec{r})=\rho_0(\vec{r})} = 0. \tag{1.5}$$

In particular DFT is also valid for systems which are inhomogeneous on a microscopic scale. In principle, all fluctuations are included in an external potential which breaks all symmetries. For interacting systems in 3d, however, $\Omega(T,\mu,[\rho])$ is not known.

Fortunately, there are few exceptions where the density functional is known exactly. First, for low density, the ideal-gas-limit is reached and the density functional can be constructed analytically (see below). Next leading orders for finite densities can be incorporated via a virial expansion which is quadratic in the densities. Conversely, in the high-density-limit, the mean-field approximation (see below) becomes asymptocially exact for penetrable potentials.
Indeed this approximation also works surprisingly well for finite densities beyond overlap. Furthermore, the density functional is exactly known (as so-called Percus-functional) in one spatial dimension for the Tonks gas (had rods on a line). However, the latter system does not exhibit freezing. Please note that the knowledge of a functional is much more than a bulk equation of state since it can be applied to any external potential $V_{ext}(\vec{r})$.

In principle, the application of DFT to freezing works as follows: First one has to chose an approximation. Then the density field is parameterized with variational parameters. In the homogeneous gas and liquid bulk phase one takes

$$\rho(\vec{r}) = \bar{\rho} \tag{1.6}$$

where $\bar{\rho}$ is a variational parameter. On the other hand, for the solid, the Gaussian approximation of density peaks on the lattice positions is an excellent choice [24].

$$\rho(\vec{r}) = \left(\frac{\alpha}{\pi}\right)^{-3/2} \sum_n \exp\left(-\alpha\left(\vec{r}-\vec{R}_n\right)^2\right) \tag{1.7}$$

Here both the lattice structure and spacing as well as the width α are variational parameters. Finally, for a given chemical potential μ and temperature T, one has to minimize the functional $\Omega(T,\mu,[\rho])$ with respect to

all variational parameters. As a result one obtains the phase diagram in the μT plane.

The procedure itself is sketched close to the solid-liquid transition in Figures 1.5 and 1.6. A solid-liquid transition line in the μT plane is schematically shown in Figure 1.5 and we consider a path with fixed μ and increasing T crossing the solid-liquid transition at $\mu = \mu_{coex}$ and $T = T_{coex}$. Coexistence implies that temperature T, chemical potential μ and pressure p are the same in both phases. Since in the bulk $p = -\Omega/V$ (V denoting the system volume) coexistence means that at given μ and T, Ω/V has two minima with equal depth. A contour plot of the density functional in the space of variational parameters is shown in Figure 1.6 for three different temperature on the path shown in Figure 1.5. The liquid minimum occurs at zero α while the solid is characterized by a minimum at finite α. The global minimum is the stable phase and at coexistence, the two minima have equal depth.

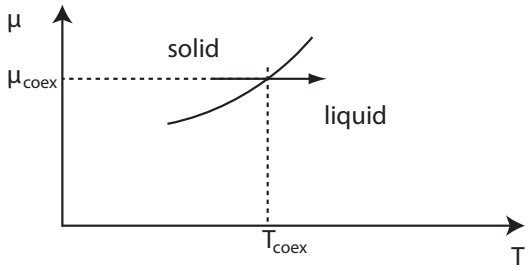

Fig. 1.5. Solid-liquid coexistence line in the μT plane. The path along which three state points are discussed in Figure 1.6 is indicated.

b) Approximations for the density functional

Let us first recall the exact functional for the ideal gas where $V(r) = 0$. It reads as

$$\mathcal{F}_{\rm id}(T,[\rho]) = k_B T \int {\rm d}^3 r \ \rho(\vec{r}) \left[\ln(\rho(\vec{r})\Lambda^3) - 1\right] \tag{1.8}$$

and minimization

$$\left.\frac{\delta \mathcal{F}_{\rm id}}{\delta \rho(\vec{r})}\right|_0 = k_B T \ln(\rho(\vec{r})\Lambda^3) + V_{\rm ext}(\vec{r}) - \mu \tag{1.9}$$

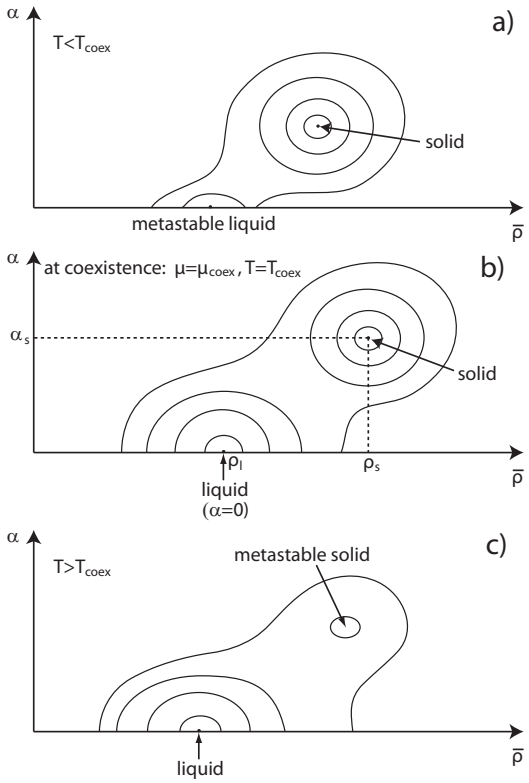

Fig. 1.6. Contour plot of the grandcanonical free energy $\Omega(T, \mu, \bar{\rho}, \alpha)$ for fixed T and μ as a function of two variational parameters α and the averaged density $\bar{\rho}$. The latter is given by the lattice constant in the solid phase. a) with a stable solid phase, b) at solid-liquid coexistence, c) with a stable liquid phase.

leads to the generalized barometric law

$$\rho_0(\vec{r}) = \frac{1}{\Lambda^3} \exp\left(-\frac{V_{\text{ext}}(\vec{r}) - \mu}{k_B T}\right) \tag{1.10}$$

for the inhomogenous density. In the interacting case, $V(r) \neq 0$, one can split

$$\mathcal{F}(T, [\rho]) =: \mathcal{F}_{\text{id}}(T, [\rho]) + \mathcal{F}_{\text{exc}}(T, [\rho]) \tag{1.11}$$

which defines the excess free energy density functional $\mathcal{F}_{exc}(T, [\rho])$. Approximations work on different levels. In the *mean-field approximation*, we

set

$$\mathcal{F}_{\rm exc}(T,[\rho]) \approx \frac{1}{2}\int {\rm d}^3r \int {\rm d}^3r'\, V(|\vec{r}-\vec{r}'|)\rho(\vec{r})\rho(\vec{r}') \tag{1.12}$$

In fact, the mean-field approximation (together with a correlational hole in the solid) yields freezing of the Gaussian potential [25] and is the correct starting point for cluster crystals for penetrable potentials [23].

The Ramakrishnan-Yussouff (RY) approximation is a perturbative treatment out of the bulk liquid which needs the bulk liquid direct correlation function $c^{(2)}(r,\bar{\rho},T)$ as an input. A functional Taylor expansion around a homogeneous reference density up to second order yields

$$\mathcal{F}_{\rm exc}(T,[\rho]) \cong -\frac{k_BT}{2}\int {\rm d}^3r \int {\rm d}^3r'\;\; c^{(2)}(|\vec{r}-\vec{r}'|,\bar{\rho},T)(\rho(\vec{r})-\bar{\rho})(\rho(\vec{r}')-\bar{\rho}) \tag{1.13}$$

The RY approximation leads to freezing for hard spheres and was historically the first demonstration that freezing can be described within DFT. The RY functional can readily be generalized to soft interactions [26] (as the OCP) and gives reasonable results for freezing there (though it is better to improve the functional by including triplet correlations).

A non-perturbative functional is based on Rosenfeld's fundamental measure theory (FMT). This works, however, only for hard spheres. In FMT we have

$$\frac{\mathcal{F}_{\rm exc}[\rho]}{k_BT} = \int {\rm d}^3r\;\; \Phi[\{n_\alpha(\vec{r})\}] \tag{1.14}$$

with

$$n_\alpha(\vec{r}) = \int {\rm d}^3r'\;\; w^{(\alpha)}(\vec{r}-\vec{r}')\rho(\vec{r}') \tag{1.15}$$

where the six weight function are given explicitly as

$$w^{(0)}(\vec{r}) = \frac{w^{(2)}(\vec{r})}{\pi\sigma^2} \tag{1.16}$$

$$w^{(1)}(\vec{r}) = \frac{w^{(2)}(\vec{r})}{2\pi\sigma} \tag{1.17}$$

$$w^{(2)}(\vec{r}) = \delta\left(\frac{\sigma}{2} - r\right) \tag{1.18}$$

$$w^{(3)}(\vec{r}) = \Theta\left(\frac{\sigma}{2} - r\right) \tag{1.19}$$

$$w^{(V_1)}(\vec{r}) = \frac{\vec{w}^{(V_2)}(\vec{r})}{2\pi\sigma} \tag{1.20}$$

$$w^{(V_2)}(\vec{r}) = \frac{\vec{r}}{r}\delta\left(\frac{\sigma}{2} - r\right) \tag{1.21}$$

with σ denoting the hard sphere diameter and

$$\Phi = \Phi_1 + \Phi_2 + \Phi_3 \tag{1.22}$$

$$\Phi_1 = -n_0 \ln(1 - n_3) \tag{1.23}$$

$$\Phi_2 = \frac{n_1 n_2 - \vec{n}_{v_1} \cdot \vec{n}_{v_2}}{1 - n_3} \tag{1.24}$$

$$\Phi_3 = \frac{\frac{1}{3}n_2^3 - n_2(\vec{n}_{v_2} \cdot \vec{n}_{v_2})}{8\pi(1 - n_3)^2} \tag{1.25}$$

This FMT functional yields the Percus-Yevick solution of the direct correlation function as an output. It furthermore survives the dimensional crossover [27]: If the three-dimensional hard sphere system is confined within a one-dimensional tube, the exact Percus functional is recovered. Moreover, in a spherical cavity which holds one or no particle at all, the exact functional is recovered. This helps to understand that the constraint packing argument of freezing is geometrically included in the FMT. In fact (also with a tensor modification in Φ_3 [28]), the FMT gives excellent data for hard-sphere freezing [27], see Table 1.1 and the recent review by Roth [9].

Table 1.1. Coexisting number densities and solid Lindemann parameter at coexistence for the hard sphere systems. "Exact" computer simulation data are shown as well as DFT data using the Ramakrishnan-Yussouff (RY) or Rosenfeld's fundamental measure theory.

	$\rho_l\ \sigma^3$	$\rho_s\ \sigma^3$	L (: Lindemann)
computer simulations	0.94	1.04	0.129
RY	0.97	1.15	0.06
Rosenfeld	0.94	1.03	0.101

Last but not least we mention perturbation theories which can be used for attractive tails. The total potential $V(r)$ is then split into a purely repulsive short-ranged part $V_{rep}(r)$ and a longer-ranged attractive part $V_{attr}(r)$ such that $V(r) = V_{rep}(r)+V_{attr}(r)$. The repulsive part is treated as an effective hard core with an effective (temperature-dependent) Barker-Henderson diameter

$$\sigma(T) = \int_0^\infty \mathrm{d}r \ \left(1 - e^{-\beta V_{\mathrm{rep}}(r)}\right) \tag{1.26}$$

and the attractive part is treated within mean-field approximation. Accordingly, the total excess free energy functional reads as

$$\begin{aligned}\mathcal{F}_{\mathrm{exc}}(T,[\rho]) \cong \mathcal{F}_{\mathrm{exc}}^{\mathrm{HS}}(T,[\rho])\big|_{\sigma=\sigma(T)} \\ + \frac{1}{2}\int \mathrm{d}^3 r \int \mathrm{d}^3 r' \ \rho(\vec{r})\rho(\vec{r}')V_{\mathrm{attr}}(|\vec{r}-\vec{r}'|)\end{aligned} \tag{1.27}$$

This procedure yields good phase diagrams for both Lennard-Jones potentials and sticky-hard-sphere systems including the isostructural solid-solid transition [18].

To summarize:

(1) Rosenfelds FMT yields excellent data for hard sphere freezing.
(2) The much less justified RY perturbative approach works in principle for softer repulsions.
(3) The mean-field density functional approximation works for penetrable potentials.
(4) Hard sphere pertubation theory yields stability of liquids and solid-solid isostructural transitions.

2. Brownian Dynamics

2.1. *Brownian dynamics (BD)*

Colloidal particles are embedded in a molecular solvent and are therefore randomly kicked by the solvent molecules on timescales much smaller than the drift of the colloidal motion [5, 29].

Let us first discuss the Smoluchowski picture. Here the time-dependent density field is the central quantity. It should follow a simple deterministic diffusion equation. For noninteracting particles with an inhomogeneous time-dependent particle density $\rho(\vec{r},t)$, Ficks law states that the current density $\vec{j}(\vec{r},t)$ is

$$\vec{j}(\vec{r},t) = -D_0 \vec{\nabla} \rho(\vec{r},t) \tag{1.28}$$

where D_0 is a phenomenological diffusion coefficient.

The continuity equation of particle conservation

$$\frac{\partial \rho(\vec{r},t)}{\partial t} + \vec{\nabla} \cdot \vec{j}(\vec{r},t) = 0 \tag{1.29}$$

then leads to the wellknown diffusion equation for $\rho(\vec{r},t)$:

$$\frac{\partial \rho(\vec{r},t)}{\partial t} \equiv D_0 \Delta \rho(\vec{r},t) \tag{1.30}$$

In the presence of an external potential $V_{\rm ext}(\vec{r})$, the force $\vec{F} = -\vec{\nabla} V_{\rm ext}(\vec{r})$ acts on the particles and will induce a drift velocity $\vec{v}_{\rm D}$ resp. an additional current density

$$\vec{j}_{\rm D} = \rho \vec{v}_{\rm D} \ . \tag{1.31}$$

We now assume totally overdamped motion since inertia effects are small as the colloids are much bigger than the solvent molecules. This results in

$$\vec{v}_{\rm D} = \frac{\vec{F}}{\xi} = -\frac{1}{\xi} \vec{\nabla} V_{\rm ext}(\vec{r}) \tag{1.32}$$

with ξ denoting a friction coefficient. For a sphere of radius R in a viscous solvent, $\xi = 6\pi\eta_{\rm s} R$, with $\eta_{\rm s}$ denoting the shear viscosity of the solvent (Stokes law). Now the total current density is

$$\vec{j} = -D_0 \vec{\nabla} \rho(\vec{r},t) - \rho(\vec{r},t) \frac{1}{\xi} \vec{\nabla} V_{\rm ext}(\vec{r}) \tag{1.33}$$

In equilibrium, the one-particle density is a Boltzmann distribution

$$\rho(\vec{r},t) \equiv \rho^{(1)}(\vec{r}) = \rho^{(0)}(\vec{r}) = A \exp(-\beta V_{\rm ext}(\vec{r})) \tag{1.34}$$

Futhermore, in equilibrium, the total current has to vanish. Therefore, necessarily

$$D_0 = \frac{k_B T}{\xi} \tag{1.35}$$

which is the socalled Stokes-Einstein relation. Hence $\vec{j} = -\frac{1}{\xi}(k_BT\vec{\nabla}\rho + \rho\vec{\nabla}V_{\rm ext})$ and the continuity equation yields

$$\frac{\partial\rho(\vec{r},t)}{\partial t} = \frac{1}{\xi}(k_BT\Delta\rho(\vec{r},t) + \vec{\nabla}(\rho(\vec{r},t)\vec{\nabla}V_{\rm ext}(\vec{r}))) \tag{1.36}$$

which is called Smoluchowski equation (for non-interacting particles).
The same equation holds for the probability density $w(\vec{r},t)$ to find a particle at position $\vec{r}$ for time t. For N non-interacting particles,

$$w(\vec{r},t) = \frac{1}{N}\rho(\vec{r},t)\ , \tag{1.37}$$

and the Smoluchowski equation reads:

$$\frac{\partial w}{\partial t} = \frac{1}{\xi}(k_BT\Delta w - \vec{\nabla}(w\cdot\vec{\nabla}V_{\rm ext})) \tag{1.38}$$

Now we consider N **interacting** particles. Using a compact notation for the particle positions

$$\{x_i\} = \{\vec{r}_i\} = \{\underbrace{x_1,x_2,x_3}_{\vec{r}_1},\underbrace{x_4,x_5,x_6}_{\vec{r}_2},\cdots,\underbrace{x_{3N-2},x_{3N-1},x_{3N}}_{\vec{r}_N}\} \tag{1.39}$$

we assume a linear relation between acting forces on the particles and the resulting drift velocities. (The same compact notation is used for other multiple vectors.) The details of this relation embody the socalled hydrodynamic interations mediated between the colloidal particles by the solvent flow field induced by the moving colloidal particles. This linear relation is in general

$$v_i = \sum_{j=1}^{3N} L_{ij}(\{x_n\})\vec{F}_j \tag{1.40}$$

where $\vec{F}_j = -\frac{\partial}{\partial x_j}U_{\rm tot}$ where $U_{\rm tot}$ involves both the internal and the interaction potential energy and v is the drift velocity. The underlying assumption in (1.40) is that the hydrodynamic interactions act quasi-instantaneously. This is justified by the fact that the timescale upon which a shear perturbation is traveling through the suspension within an interparticle distance is much smaller than that of Brownian motion. The coefficients L_{ij} constitute the socalled $3N\times 3N$ mobility matrix and can in principle be obtained by solving the Navier-Stokes equations of N spheres with appropriate stick boundary conditions of the solvent flow field on the particle's surfaces.

In general, L_{ij} depends on $\vec{r}^N$, and we postulate:

symmetry

$$L_{ij} = L_{ji} \tag{1.41}$$

positivity

$$\sum_{ij} F_i F_j L_{ij} > 0 \text{ for all } F_{i,j} \neq 0 \tag{1.42}$$

With $w(\{\vec{r}_i\}, t)$ denoting the probability density for interacting particles, the suitable generalization of the continuity equation is

$$\frac{\partial w}{\partial t} = -\sum_{n=1}^{3N} \frac{\partial}{\partial x_n}(v_{\mathrm{tot},n} w) \tag{1.43}$$

with

$$v_{\mathrm{tot},n} = \sum_{m=1}^{3N} L_{mn} \frac{\partial}{\partial x_m}(k_B T \ln w + U_{\mathrm{tot}}) \tag{1.44}$$

which leads to the generalized Smoluchowski equation fo interacting particles.

$$\frac{\partial w}{\partial t} = \hat{\mathcal{O}} w \tag{1.45}$$

with the Smoluchwoski operator

$$\hat{\mathcal{O}} = \sum_{n,m=1}^{3N} \frac{\partial}{\partial x_n} L_{nm} (k_B T \frac{\partial}{\partial x_m} + \frac{\partial U_{\mathrm{tot}}}{\partial x_m}) \tag{1.46}$$

In many applications, hydrodynamic interactions are neglected. This means that the mobility matrix is constant and a diagonal

$$L_{nm} = \frac{1}{\xi} \delta_{nm} \tag{1.47}$$

This assumption, however, is only true for small volume fraction of the colloidal particles.

Complementary to the Smoluchowski approach which considers diffusion in phase space, stochastic trajectories in real-space are the basic ingredients for the Langevin picture. A typical "cuspy" Brownian trajectories of a colloidal particle is shown in Figure 1.7

First, we consider only one particle in an external potential $V_{\mathrm{ext}}(\vec{r})$ with random force $\vec{f}(t)$. The stochastic differential equation for a single particle is completely overdamped

$$\xi \dot{\vec{r}} = -\vec{\nabla} V_{\mathrm{ext}}(\vec{r}) + \vec{f}(t) \tag{1.48}$$

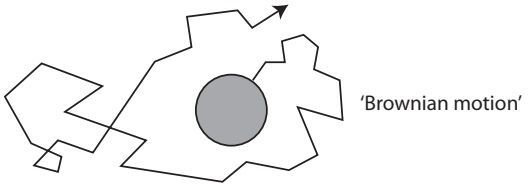

Fig. 1.7. Typical trajectory of a randomly kicked Brownian particle.

where $\vec{f}(t)$ mimicks the random kicks of the solvent and is a Gaussian random variable which fulfills

$$\langle \vec{f}(t) \rangle = 0 \tag{1.49}$$

$$\langle f_i(t) f_j(t') \rangle = 2\xi k_B T \delta_{ij} \delta(t - t') \tag{1.50}$$

One can show that this is stochastically equivalent to the Smoluchowski equation of non-interacting particles. For interacting particles, the Smoluchowski equation is obtained from the following Langevin equations [5]:

$$\dot{x}_n(t) = \sum_{m=1}^{3N} L_{nm}(-\frac{\partial U_{\rm total}}{\partial x_m} + f_m(t)) + k_B T \sum_{m=1}^{3N} \frac{\partial L_{nm}}{\partial x_m} \tag{1.51}$$

with Gaussian random variables f_m which fulfill

$$\langle \vec{f_m}(t) \rangle = 0 \tag{1.52}$$

$$\langle f_m(t) f_{m'}(t') \rangle = 2L^{-1}_{mm'} k_B T \delta(t - t'). \tag{1.53}$$

2.2. *BD computer simulations*

In Brownian Dynamic (BD) computer simulations we use the overdamped Langevin equation (1.48) with a single realization of the stochastic process. Applying this to a finite time step Δt and integrating

$$x_n(t + \Delta t) = x_n(t) + \Delta t \sum_{m=1}^{3N} L_{nm}(-\frac{\partial U_{\rm total}}{\partial x_m}) + \Delta_n + k_B T \Delta t \sum_m \frac{\partial L_{nm}}{\partial x_m}$$

$$\text{where} \quad \Delta_n = \int_t^{t+\Delta t} \mathrm{d}t' \sum_m L_{nm} f_m(t') \quad \text{is Gaussian distributed}$$

and possesses the moments

$$\langle \Delta_n \rangle = \int_t^{t+\Delta t} \mathrm{d}t' \sum_m L_{nm} \langle f_m(t') \rangle = 0$$

$$\langle \Delta_n \Delta_{n'} \rangle = 2 k_B T \Delta t L_{nn'},$$

which is the basic equation for BD computer simulations. For each step we need to generate a Gaussian random number and update the Langevin equation by calculating $x_n(t+\Delta t)$. Although this algorithm is less efficient than MD/MC for equilibrium correlations, it is unavoidable for calculation of colloidal dynamics.

2.3. *Dynamical density functional theory (DDFT)*

Here we derive a deterministic equation for the time-dependent one-particle density from the Smoluchowski equations [25]. We follow the idea of Archer and Evans [30]. First, we recall Smoluchowski equation for the N-particle density

$$w(\vec{r}_1,\ldots,\vec{r}_N,t) \equiv w(\vec{r}^N,t) \quad , \quad \vec{r}^N = \{\vec{r}_1,\ldots,\vec{r}_N\} \text{ as}$$

$$\frac{\partial w}{\partial t} = \hat{\mathcal{O}} w = \frac{1}{\xi}\sum_{i=1}^{N} \vec{\nabla}_i \cdot [k_B T \vec{\nabla}_i + \vec{\nabla}_i U_{\text{tot}}(\vec{r}^N,t)] w \tag{1.54}$$

with

$$U_{\text{tot}}(\vec{r}^N,t) = \sum_{i=1}^{N} V_{\text{ext}}(\vec{r}_i,t) + \sum_{\substack{i,j=1 \\ i<j}}^{N} V(|\vec{r}_i - \vec{r}_j|) \tag{1.55}$$

Here, hydrodynamic interactions have been neglected. Now the idea is to integrate out degrees of freedom. In fact, an integration yields

$$\rho(\vec{r}_1,t) = N \int \mathrm{d}^3 r_2 \ldots \int \mathrm{d}^3 r_N \; w(\vec{r}^N,t) \tag{1.56}$$

The 2-particle density is analogously obtained as

$$\rho^{(2)}(\vec{r}_1,\vec{r}_2,t) = N(N-1) \int \mathrm{d}^3 r_3 \ldots \int \mathrm{d}^3 r_N \; w(\vec{r}^N,t) \tag{1.57}$$

Integrating the Smoluchowski equation with $N \int \mathrm{d}^3 r_2 \ldots \int \mathrm{d}^3 r_N$ yields

$$\begin{aligned} \xi \frac{\partial}{\partial t}\rho(\vec{r}_1,t) = {} & k_B T \Delta_1 \rho(\vec{r}_1,t) + \vec{\nabla}_1 (\rho(\vec{r}_1,t) \vec{\nabla}_1 V_{\text{ext}}(\vec{r}_1,t) \\ & + \vec{\nabla}_1 \int \mathrm{d}^3 r_2 \; \rho^{(2)}(\vec{r}_1,\vec{r}_2,t) \vec{\nabla}_1 V(|\vec{r}_1 - \vec{r}_2|) \end{aligned} \tag{1.58}$$

In equilibrium, necessarily $\frac{\partial \rho(\vec{r}_1,t)}{\partial t} = 0$ which implies

$$0 = \vec{\nabla}\left(k_B T \vec{\nabla}\rho(\vec{r}) + \rho(\vec{r}) \vec{\nabla} V_{\text{ext}}(\vec{r}) + \int \mathrm{d}^3 r' \; \rho^{(2)}(\vec{r},\vec{r}\,') \vec{\nabla} V(|\vec{r} - \vec{r}\,'|) \right) \tag{1.59}$$

The constant must vanish for $r \to \infty$ and is thus identical to zero. Therefore

$$0 = k_B T \vec{\nabla} \rho(\vec{r}) + \rho(\vec{r}) \vec{\nabla} V_{\rm ext}(\vec{r}) + \int {\rm d}^3 r' \ \rho^{(2)}(\vec{r}, \vec{r}') \vec{\nabla} V(|\vec{r} - \vec{r}'|) \quad (1.60)$$

This is also known as Yvon-Born-Green-hierarchy (YBG).

In equilibrium, DFT implies:

$$\frac{\delta \mathcal{F}}{\delta \rho(\vec{r})} = \mu - V_{\rm ext}(\vec{r}) \quad (1.61)$$

$$= k_B T \ln(\Lambda^3 \rho(\vec{r})) + \frac{\delta \mathcal{F}_{\rm exc}}{\delta \rho(\vec{r})} \text{ , since } \mathcal{F} = \mathcal{F}_{\rm id} + \mathcal{F}_{\rm exc} \quad (1.62)$$

We now apply the gradient which gives:

$$\vec{\nabla} V_{\rm ext}(\vec{r}) + k_B T \vec{\nabla} \ln(\Lambda^3 \rho(\vec{r})) + \vec{\nabla} \frac{\delta \mathcal{F}_{\rm exc}}{\delta \rho(\vec{r})} = 0 \quad (1.63)$$

combined with YBG we obtain

$$\int {\rm d}^3 r' \ \rho^{(2)}(\vec{r}, \vec{r}') \vec{\nabla} V(|\vec{r} - \vec{r}'|) = \rho(\vec{r}) \vec{\nabla} \cdot \frac{\delta \mathcal{F}_{\rm exc}[\rho]}{\delta \rho(\vec{r})} \quad (1.64)$$

We postulate that this argument holds also in nonequilibrium. In doing so, non-equilibrium correlations are approximated by equilibrium ones at the same $\rho(\vec{r}, t)$ (via a suitable $V_{\rm ext}(\vec{r})$ in equilibrium). Equivalently, one can say that it is postulated that pair correlations decay much faster to their equilibrium one than the one-body density. Therefore the basic approximation of DDFT is sometimes called adiabatic approximation. (For an alternate derivation, see Marconi and Tarazona [31, 32] or Español and Löwen [33].)

Hence:

$$\xi \frac{\partial \rho(\vec{r}, t)}{\partial t} = \vec{\nabla} (k_B T \vec{\nabla} \rho(\vec{r}, t) + \rho(\vec{r}, t) \vec{\nabla} V_{\rm ext}(\vec{r}, t) + \rho(\vec{r}, t) \vec{\nabla} \frac{\delta \mathcal{F}_{\rm exc}}{\delta \rho(\vec{r}, t)}) \quad (1.65)$$

or equivalently

$$\boxed{\xi \frac{\partial \rho(\vec{r}, t)}{\partial t} = \vec{\nabla} \rho(\vec{r}, t) \vec{\nabla} \frac{\delta \Omega[\rho]}{\delta \rho(\vec{r}, t)}} \quad (1.66)$$

which constitutes the basic equation of dynamical density functional theory (DDFT).

The applications of DDFT are numerous. The dynamics of a strongly inhomogeneous Brownian fluid has found to be a good agreement with BD computer simulations. [34, 35]

2.4. *An example: Crystal growth at imposed nucleation clusters*

The dynamical density functional theory can also be used for the dynamics of the crystal. This is demonstrated by an example in the following. A two-dimensional system with the repulsive inverse power-law potential $V(r) = V_0/r^3$ corresponds to dipoles in a plane whose dipole moments are perpendicular to the plane. Two-dimensional systems are best realized for superparamagnetic colloids pending at an air-water interface in an external magnetic field [36, 37]. The RY functional gives a reasonable description for the two-dimensional crystallization [26].

The dynamical version can be applied to a situation where a cluster of 19 particles from a prescribed cut-out of a triangular lattice is imposed and offered as a nucleation seed to an undercooled fluid. This cluster is first fixed and then instantaneously released. Depending on the lattice constant of the prescribed nucleation cluster, there is either subsequent crystal growth or relaxation back to the undercooled fluid. Two examples are shown in Figure 1.8. The one-particle density field is shown for fixed time as a contour plot. In both examples, the crystalline seed is compressed relative to the stable bulk one. If the compression is significant but not too large (Figure 1.8, left panel), there is still crystal growth, but if the crystal is compressed further, the seed is too dissimilar to the bulk crystal as to initiate crystal growth (Figure 1.8, right panel). The same qualitative behaviour has been found in Brownian dynamics computer simulations [38].

This example shows that dynamical density functional theory represents a reliable microscopic approach to nonequilibrium phenomena like crystal growth in an external field [39]. A similar behaviour has been seen for growing crystal fronts [38, 40] and for vacancy dynamics in two-dimensional solids.

2.5. *Hydrodynamic interactions*

Here we address the question how $L_{nm}(\{x_j\})$ looks like explicitely. Solving the linearized Navier-Stokes equations with the appropiate stick boundary

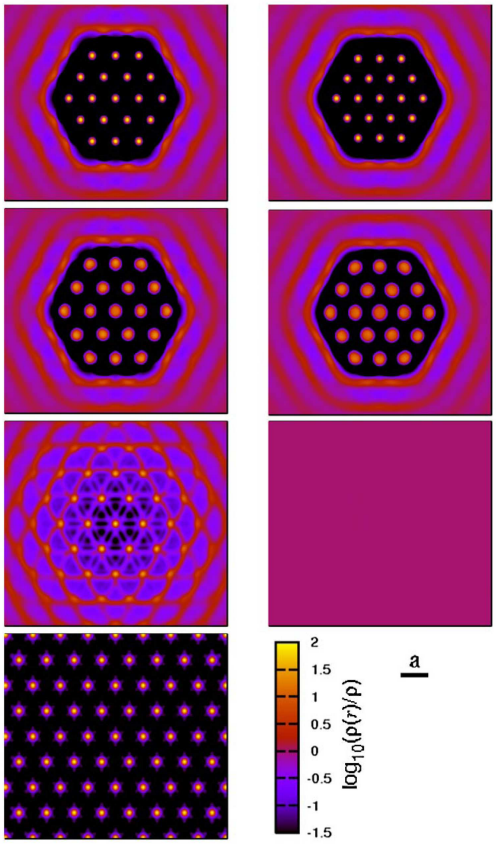

Fig. 1.8. Snapshots of the central region of the dimensionless density field $\rho(\mathbf{r},\mathbf{t})/\rho$ of two colloidal clusters with strain parameters $A\rho = 0.7$ (left panel) and $A\rho = 0.6$ (right panel) at times $t/\tau_B = 0, 0.001, 0.1, 1.0$ (from top to bottom; $t/\tau_B = 1.0$ only for $A\rho = 0.7$). A is the area of the crystal unit cell. From [38]

.

conditions on the particle surfaces, is a difficult problem. Furthermore it is problematic that

i) $L_{nm}(\{x_j\})$ is long-ranged in terms of distances between particles
ii) H.I. have **many-body character**, pair expansion only possible at low concentrations
iii) H.I. have quite different near-field behaviour. They are divergent lubrication terms.

The linear relationship (1.40) can be rewritten as

$$\vec{v}_n = \sum_{m=1}^{N} \bar{\bar{H}}_{nm} \vec{F}_m \tag{1.67}$$

where each quantity $\bar{\bar{H}}_{nm}$ is a 3×3 matrix. In particular, we can discriminate the following cases:

1) **no H.I.** $H_{nm} = \mathbb{1} \frac{\delta_{nm}}{\xi}$

2) **Oseen-tensor**
In the Oseen approximation, $\bar{\bar{H}}_{nn} = \frac{\mathbb{1}}{\xi}$

$$\bar{\bar{H}}_{nm} = \bar{\bar{H}}(\underbrace{\vec{r}_n - \vec{r}_m}_{\vec{r}}) \text{ for } n \neq m \tag{1.68}$$

with the Oseen tensor

$$\bar{\bar{H}}(\vec{r}) = \frac{1}{8\pi\eta_s}(\mathbb{1} + \hat{r} \otimes \hat{r})\frac{1}{r} \quad , \quad \hat{r} = \frac{\vec{r}}{r} \tag{1.69}$$

This is the leading far field term for two particles at large distance $\vec{r}$. The symbol $\otimes$ denotes the dyadic product or tensor product.

3) **Rotne-Prager-tensor**
In this approximation, the next leading correction is included.

$$H_{nn} = \frac{\mathbb{1}}{\xi}, \quad H_{nm} = \bar{\bar{H}}_{RP}(\vec{r}_n - \vec{r}_m) \tag{1.70}$$

with

$$\bar{\bar{H}}_{RP}(\vec{r}) = \frac{D_0}{k_B T}\left(\frac{3}{4}\frac{R_H}{r}[\mathbb{1} + \hat{r} \otimes \hat{r}] + \frac{1}{2}\frac{R_H^3}{r^3}[1 - 3\hat{r} \otimes \hat{r}]\right) \tag{1.71}$$

Higher order expansions of higher order than $\frac{1}{r^3}$ are possible. These include also terms of sphere rotation. Finally the triplet contribution can be estimated.

The DDFT can be generalized to hydrodynamic interactions [41]. Again the starting point is the Smoluchowski equation which we now write in the form

$$\frac{\partial w(\vec{r}^N, t)}{\partial t} = \sum_{i,j=1}^{N} \vec{\nabla}_i \cdot \bar{\bar{H}}_{ij}(\vec{r}^N) \cdot \left[\vec{\nabla}_j + \vec{\nabla}_j \frac{U_{\text{tot}}(\vec{r}^N, t)}{k_B T}\right] w(\vec{r}^N, t) \tag{1.72}$$

We use the two particle approximation

$$\bar{\bar{H}}_{ij}(\vec{r}^N) \approx \frac{D_0}{k_B T}\left(\mathbb{1}\delta_{ij} + \delta_{ij}\sum_{i\neq j}\omega_{11}(\vec{r}_i - \vec{r}_e) + (1-\delta_{ij})\omega_{12}(\vec{r}_i - \vec{r}_e)\right) \tag{1.73}$$

on the level of the Rotne-Prager expression

$$\omega_{11}(\vec{r}) = 0 \tag{1.74}$$

$$\omega_{12}(\vec{r}) = \frac{3}{8}\frac{\sigma_H}{r}(\mathbb{1} + \hat{r}\otimes\hat{r}) + \frac{1}{16}(\frac{\sigma_H}{r})^3(1 - 3\hat{r}\otimes\hat{r}) + O((\frac{\sigma_H}{r})^7) \tag{1.75}$$

where σ_H is the hydrodynamic diameter.

Integrating Smoluchowski equation [25] then yields [41]

$$\begin{aligned}\frac{k_B T}{D_0}\frac{\partial\rho(\vec{r},t)}{\partial t} = \nabla_r\cdot\Big[&\rho(\vec{r},t)\nabla_r\frac{\delta\mathcal{F}[\rho]}{\delta\rho(\vec{r},t)} \\ &+ \int \mathrm{d}\vec{r}'\ \rho^{(2)}(\vec{r},\vec{r}',t)\omega_{11}(\vec{r}-\vec{r}')\cdot\nabla_r\frac{\delta\mathcal{F}[\rho]}{\delta\rho(\vec{r},t)} \\ &+ \int \mathrm{d}\vec{r}'\ \rho^{(2)}(\vec{r},\vec{r}',t)\omega_{12}(\vec{r}-\vec{r}')\cdot\nabla_r\frac{\delta\mathcal{F}[\rho]}{\delta\rho(\vec{r},t)}\Big]\end{aligned} \tag{1.76}$$

A possible closure is via the Ornstein-Zernike equation

$$\begin{aligned}\rho^{(2)}(\vec{r},\vec{r}',t) = &(1 + c^{(2)}(\vec{r},\vec{r}'))\rho(\vec{r},t)\rho(\vec{r}',t) \\ &+ \rho(\vec{r}',t)\int \mathrm{d}\vec{r}''((\rho^{(2)}(\vec{r},\vec{r}'',t) - \rho(\vec{r},t)\rho(\vec{r}'',t))c^{(2)}(\vec{r}'',\vec{r}'))\end{aligned} \tag{1.77}$$

with

$$c^{(2)}(\vec{r},\vec{r}') = -\beta\frac{\delta^2\mathcal{F}_{\mathrm{exc}}[\rho]}{\delta\rho(\vec{r},t)\delta\rho(\vec{r}',t)} \tag{1.78}$$

In an easier attempt, one can approximate

$$\rho^{(2)}(\vec{r},\vec{r}',t) \approx \rho(r,t)\rho(r',t)g(|\vec{r}-\vec{r}'|,\bar{\rho}) \tag{1.79}$$

where $\bar{\rho}$ is a suitable averaged density and $g(r,\bar{\rho})$ is a pair distribution function in the equilibrium bulk fluid.

Finally we describe an example which involves hard sphere colloids of diameter σ moving in a time-dependent oscillating radial-symmetric trapping potential $V_{\mathrm{ext}}(r,t)$. The potential reads as

$$V_{\mathrm{ext}}(r,t) = V_1 r^4 + V_2\cos(\omega t)r^4 \tag{1.80}$$

and corresponds to a shape which switches between stable and unstable situations at the origin $r = 0$ but is globally stable. The amplitudes are $V_1 = 10k_BT/4096\sigma^4$, $V_2 = k_BT/\sigma^2$ and the external switching frequency is $\omega = 4\pi D_0/\sigma^2$. As a result, the density profile is picking up the external frequency ω and exhibits a breathing mode, i.e. it is periodically expanding and compressed again by the external potential (1.80). Time-dependent density profiles $\rho(r,t)$ are presented in Figure 1.9 in the steady breathing state.

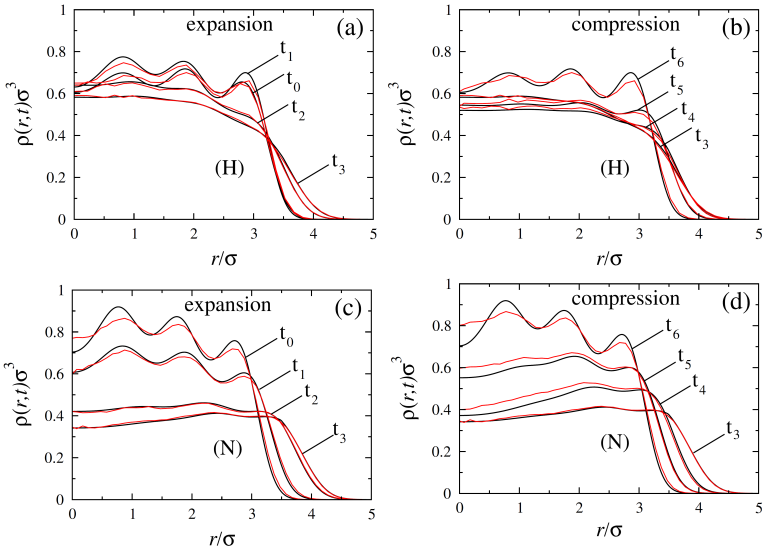

Fig. 1.9. *Steady-state* DDFT (solid curves) and BD (noisy curves) results for the time-dependent density profile $\rho(r,t)$. In Fig. (a) and (b) hydrodynamic interactions are taken into account while in (c) and (d) they are neglected. (a) and (c) correspond to the expanding half period and (b) and (d) to the compressing half period, respectively. The profiles correspond to the following time sequence: $t_0 = 2.5\tau_B$, $t_1 = 2.6\tau_B$, $t_2 = 2.7\tau_B$, $t_3 = 2.75\tau_B$ in (a) and (c), and $t_3 = 2.75\tau_B$, $t_4 = 2.85\tau_B$, $t_5 = 2.9\tau_B$ and $t_6 = 3.0\tau_B$, $\tau_B = \sigma^2/D_0$. From Ref. [41].

Figures 1.9(a) and (b) show results for hydrodynamic interactions included on the Rotne-Prager level. DDFT data are in very good agreement with Brownian dynamics computer simulations which include hydrodynamic interactions on the same Rotne-Prager level. On the other hand, in Figure 1.9(c) and (d), hydrodynamic interactions are ignored. The density profiles are qualitatively different to that shown in Figures 1.9(a) and

(b) but again DDFT data are in agreement with Brownian dynamics computer simulations. This demonstrates that DDFT is a reliable microscopic theory both if hydrodynamic interactions are included or ignored.

3. Rod-like particles

3.1. *Statistical mechanics of rod-like particles*

Density functional theory can readily be extended to rod-like particles which possess an additional orientational degree of freedom described by a unit vector $\hat{u}$. A configuration of N particles is now fully specified by the set of positions of the center of masses and the corresponding orientations $\{\vec{R}_i, \hat{u}_i, i = 1, \ldots, N\}$, see Figure 1.10.

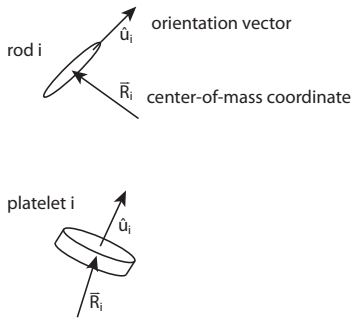

Fig. 1.10. Sketch of the center-of-mass position $\vec{R}_i$ and the orientational unit vector $\hat{u}_i$ for the i^{th} particle both for a rod-like and plate-like particle.

Example for ansiotropic particles include

(1) molecular dipolar fluids (e.g. H_2O molecule)
(2) rod-like colloids (e.g. tobacco-mosaic viruses)
(3) molecular fluids without dipole moment (apolar), (e.g. H_2 molecule)
(4) plate-like objects (clays)

The canonical partition function for rod-like particles now reads [42]

$$Z = \frac{1}{h^{6N} N!} \int\limits_V \mathrm{d}^3 R_1 \ \ldots \int\limits_V \mathrm{d}^3 R_N \int\limits_{\mathbb{R}^3} \mathrm{d}^3 p_1 \ \ldots \int\limits_{\mathbb{R}^3} \mathrm{d}^3 p_N \times \int\limits_{S_2} \mathrm{d}^2 u_1 \ \ldots \int\limits_{S_2} \mathrm{d}^2 u_N \int\limits_{\mathbb{R}^3} \mathrm{d}^3 L_1 \ \ldots \int\limits_{\mathbb{R}^3} \mathrm{d}^3 L_N \ e^{-\beta \mathcal{H}} \tag{1.81}$$

with the Hamilton function

$$\mathcal{H} = \sum_{i=1}^{N} \left\{ \frac{\vec{p}_i^2}{2m} + \frac{1}{2}\vec{L}_i(\bar{\bar{\Theta}})^{-1}\vec{L}_i \right\} + \frac{1}{2}\sum_{i,j=1}^{N} v(\vec{R}_i - \vec{R}_j, \hat{u}_i, \hat{u}_j) + \sum_{i=1}^{N} V_{\text{ext}}(\vec{R}_i, \hat{u}_i) \tag{1.82}$$

which comprises the kinetic energy, the pair interaction energy and the external energy. Here $\bar{\bar{\Theta}}$ is the inertia tensor and S_2 the unit-sphere in 3d.

Again the central quantity is the one-particle density $\rho_0^{(1)}(\vec{r}, \hat{u})$ which is defined as

$$\rho_0^{(1)}(\vec{r}, \hat{u}) := \left\langle \sum_{i=1}^{N} \delta(\vec{r} - \vec{R}_i)\delta(\hat{u} - \hat{u}_i) \right\rangle \tag{1.83}$$

Integrating the orientations over the unit sphere S_2 results in the density of the center-of-masses

$$\rho_0(\vec{r}) = \frac{1}{4\pi}\int_{S_2} \mathrm{d}^2u \ \rho_0^{(1)}(\vec{r}, \hat{u}) \tag{1.84}$$

On the other hand, the globally averaged orientational order is gained by integrating over the center-of-mass corrdinates and given by

$$f(\hat{u}) = \frac{1}{V}\int_{V} \mathrm{d}^3r \ \rho_0^{(1)}(\vec{r}, \hat{u}) \tag{1.85}$$

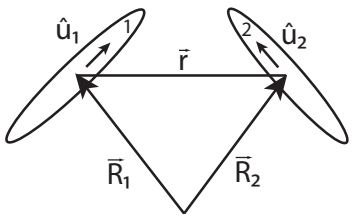

Fig. 1.11. Sketch of two interacting rods. The interaction potential depends on $\vec{r} = \vec{R}_1 - \vec{R}_2$ and $\hat{u}_1, \hat{u}_2$.

In analogy to the isotropic case, one can define a pair correlation func-

tion

$$g(\vec{R}_1,\vec{R}_2,\hat{u}_1,\hat{u}_2) := \frac{\left\langle \sum\limits_{\substack{i,j=1\\ i\neq j}}^{N} \delta(\vec{R}_1-\vec{R}_i)\delta(\vec{R}_2-\vec{R}_j)\delta(\hat{u}_1-\hat{u}_j)\delta(\hat{u}_2-\hat{u}_j)\right\rangle}{\rho_0^{(1)}(\vec{R}_1,\hat{u}_1)\rho_0^{(1)}(\vec{R}_2,\hat{u}_2)} \tag{1.86}$$

Now different phases are conceivable which can be classified and distinguished by their one-particle density field.

1) Fluid (disordered) phase, isotropic phase

Here the center-of-mass-positions and orientations are disordered:

$$\rho_0^{(1)}(\vec{r},\hat{u}) = \rho_0 = \text{const} \tag{1.87}$$

2) Nematic phase

Here, positions are disordered and orientations are ordered, i.e.

$$\rho_0^{(1)}(\vec{r},\hat{u}) = \rho f(\hat{u}) \quad , \qquad \hat{u}_0 : \text{ nematic director} \tag{1.88}$$

Typically the orientation is distributed around a nematic director $\hat{u}_0$. In order to quantify orientational order, it is convenient to introduce a nematic order parameter. In fact, this is defined via the second rank tensor

$$\bar{\bar{Q}} = \left\langle \frac{1}{N}\sum_{i=1}^{N}\left(\frac{3}{2}\hat{u}_i\otimes\hat{u}_i - \frac{1}{2}\mathbb{1}\right)\right\rangle \tag{1.89}$$

where the dyadic product is

$$\hat{u}_i\otimes\hat{u}_i = \begin{pmatrix} u_{ix}u_{ix} & u_{ix}u_{iy} & u_{ix}u_{iz} \\ u_{iy}u_{ix} & u_{iy}u_{iy} & u_{iy}u_{iz} \\ u_{iz}u_{ix} & u_{iz}u_{iy} & u_{iz}u_{iz} \end{pmatrix} \tag{1.90}$$

One can easily show that the tensor $\bar{\bar{Q}}$ is trace-less

$$\mathrm{Tr}\bar{\bar{Q}} = \frac{1}{2}\left\langle \mathrm{Tr}(3\hat{u}_i\otimes\hat{u}_i - \mathbb{1})\right\rangle \tag{1.91}$$

$$= \frac{1}{2}\left\langle 3\cdot 1 - 3\right\rangle = 0 \tag{1.92}$$

Furthermore $\bar{\bar{Q}}$ is clearly symmetric and hence diagonalizable with three eigenvalues $\lambda_1 \geq \lambda_2 \geq \lambda_3$ where λ_3 must be $-\lambda_2 - \lambda_1$. The largest eigenvalue λ_1 is called nematic order parameter S. The corresponding eigenvector is called nematic director. For perfect alignment along $\vec{u}_0$ we have

$\vec{u}_i \equiv \hat{u}_0$ for all i. Then, $S = 1$. If the two lower eigenvalues are identical, $\lambda_2 = \lambda_3$, the call it a **uniaxial nematic** phase. If $\lambda_2 \neq \lambda_3$, the orientation is called **biaxial**. In the **isotropic phase**: $S = 0$. Orientational distributions are accessible experimentally, by e.g. birefringence.

3) Smectic-A phase

The socalled smectic-A phase is positionally ordered along an orienation axis $\hat{u}_0$. The associated one-particle density is periodic in the z-direction along $\hat{u}_0$:

$$\rho_0^{(1)}(\vec{r}, \hat{u}) = \rho(z, \hat{u}) \quad z\text{-periodic} \tag{1.93}$$

4) Smectic-B phase

The smectic-B phase is similar to the smectic-A phase but exhibits an in-plane triangular lattice.

5) Columnar phase

The columnar exhibits crystalline order perpendicular to the director $\hat{u}_0$ but is disordered positionally along $\vec{u}_0$. The one-particle density field thus reads as

$$\rho_0^{(1)}(\vec{r}, \hat{u}) = \rho(x, y, \hat{u}) \tag{1.94}$$

6) Plastic crystal

In a plastic crystal, the positions are ordered in all three spatial directions but the orientations are disordered. Therefore:

$$\rho_0^{(1)}(\vec{r}, \hat{u}) = f(\vec{r}) \tag{1.95}$$

7) Full crystalline phases

Finally, in the full crystalline phase, positions and orientations are both ordered.

The list (1)-(7) of liquid crystalline phases is by far not exhaustive. There are more "exotic" phases such as an AAA stacked phase, a smectic-C with tilted rods, or cholesteric phases which possesses a helical twist with a pitch length l_p.

3.2. *Simple models*

Let us now discuss simple models for interactions between anisotropic rods. The phase behaviour of hard objects, as shown in Figure 1.12, is dominated by the shape. Temperature scales out in this case such that packing fraction alone (apart from the particle shape) is the only parameter. Hard spherocylinders have been studied, as well as hard platelets ("hard coins") or thin needles which arise from spherocylinders in the limit of infinite aspect ratio $\frac{L}{D} \to \infty$.

Fig. 1.12. Sketch of differently shaped hard bodies.

A) Analytical results by Onsager

In the limit $p = \frac{L}{D} \to \infty$, a virial expansion up to second order is getting asymptotically exact. There is a isotropic-nematic transition which can be calculated analytically [43]. It is first order with a density jump. The scaled coexistence densities of the coexisting isotropic and nematic phases are

$$\rho_{\rm iso} L^2 D = 4.189\ldots \tag{1.96}$$

and

$$\rho_{\rm nem} L^2 D = 5.376\ldots \tag{1.97}$$

At coexistence, the nematic order parameter in the nematic phase is $S = 0.784$. However, in practice, one needs pretty large aspect ratios (about $p \gtrsim 200$) in order to get reasonably into this Onsager limit.

B) Computer simulations

Full phase diagrams can be obtained by Monte Carlo computer simuations [44]. Hard spherocylinders show for various densities ρ and aspect ratios p the following stable phases: isotropic, plastic, ABC stacking, AAA stacking, smectic-A, and nematic phases. All those transitions are purely driven by entropy.

Another anisotropic system are hard ellipsoids which are characterized by two different axial lengths a and b. The phase diagram involves isotropic, nematic fully crystalline and plastic crystalline phases [45]. There is a remarkable symmetry in $x \to \frac{1}{x}$ for the topology of the phase diagram where $x = \frac{a}{b}$. $x < 1$ correspond to oblate and $x > 1$ to prolate objects.

C) Density functional theory

Again density functional theory tells us that there exists a unique grand-canonical free energy functional $\Omega(T, \mu, [\rho^{(1)}])$ (functional of the one-particle density) which becomes minimal for the equilibrium density $\rho_0^{(1)}(\vec{r}, \hat{u})$ and then equals the real grand canonical free energy, i.e.

$$\boxed{\left.\frac{\delta\Omega(T, \mu, [\rho^{(1)}])}{\delta\rho^{(1)}(\vec{r}, \hat{u})}\right|_{\rho^{(1)}=\rho_0^{(1)}(\vec{r}, \hat{u})} = 0} \tag{1.98}$$

Here, the functional can be decomposed as follows

$$\begin{aligned}\Omega(T, \mu, [\rho^{(1)}]) = k_B T \int \mathrm{d}^3 r \int \mathrm{d}^2 u \ \rho^{(1)}(\vec{r}, \hat{u})[\ln(\Lambda^3 \rho^{(1)}(\vec{r}, \hat{u})) - 1] \\ + \int \mathrm{d}^3 r \mathrm{d}^2 u \ (V_{\mathrm{ext}}(\vec{r}, \hat{u}) - \mu)\rho^{(1)}(\vec{r}, \hat{u}) + \mathcal{F}_{\mathrm{exc}}(T, [\rho^{(1)}])\end{aligned} \tag{1.99}$$

The first term on the right hand side of equation (1.99) is the functional $\mathcal{F}_{\mathrm{id}}[\rho^{(1)}]$ for ideal rotators. The excess part $\mathcal{F}_{\mathrm{exc}}(T, [\rho^{(1)}])$ is in general unknown and requires approximative treatments.

For hard spherocylinders, $\mathcal{F}_{\mathrm{exc}}(T, [\rho^{(1)}])$ can be approximated by a smoothed density approximation (SMA) [46] yielding several stable liquid-crystalline phases, namely: isotropic, nematic, smectic-A and ABC crystalline. A modified weighted density approximation (MWDA) was subsequently proposed [47] which improves upon the SMA by exhibiting stable plastic crystalline and AAA crystals as well.
An important recent progress was archieved by generalizing Rosenfeld's fundamental measure theory from hard spheres to hard objects with any shape [48]. For spherocylinders the functional was worked out explicitly. This functional could be exploited also for attractions by employing a perturbation theory for the attractive parts in the potential. Finally, a mean-field density functional for rods with soft segments was proposed and studied [49].

3.3. *Brownian dynamics of rod-like particles*

In order to derive a dynamical density functional theory (DDFT) for rod-like particles one can start from the Smoluchowski equation for the full probability density distribution $w(\vec{r}_1,\cdots,\vec{r}_N;\vec{u}_1,\cdots,\vec{u}_N,t)$ of N rods with their corresponding center-of-mass positions $\vec{r}^N=(\vec{r}_1,\cdots,\vec{r}_N)$ and orientations $\hat{u}^N=(\hat{u}_1,\cdots,\hat{u}_N)$ which reads [6]

$$\frac{\partial w}{\partial t}=\hat{\mathcal{O}}_S w \tag{1.100}$$

where the Smoluchowski operator is now given by

$$\begin{aligned}\hat{\mathcal{O}}_S=\sum_{i=1}^{N}\Bigg[&\vec{\nabla}_{\vec{r}_i}\cdot\bar{\bar{D}}(\hat{u}_i)\cdot\left(\vec{\nabla}_{\vec{r}_i}+\frac{1}{k_BT}\vec{\nabla}_{\vec{r}_i}U(\vec{r}^N,\hat{u}^N,t)\right)\\&+D_r\hat{R}_i\cdot\left(\hat{R}_i+\frac{1}{k_BT}\hat{R}_iU(\vec{r}^N,\hat{u}^N,t)\right)\Bigg]\end{aligned} \tag{1.101}$$

where $U(\vec{r}^N,\hat{u}^N,t)$ is the total potential energy. Here the rotation operator $\hat{\vec{R}}_i$ is defined as $\hat{\vec{R}}_i=\hat{u}_i\times\vec{\nabla}_{\hat{u}_i}$ and the anisotropic translational diffusion tensor is given by

$$\bar{\bar{D}}(\hat{u}_i)=D^{\shortparallel}\hat{u}_i\otimes\hat{u}_i+D^{\perp}(\vec{1}-\hat{u}_i\otimes\hat{u}_i) \tag{1.102}$$

The two diffusion constants $D^{\shortparallel}$ and $D^{\perp}$, parallel and perpendicular to the orientations reflect the fact that the translational diffusion is anisotropic. For hard spherocylinders there are valid approximations for $D^{\shortparallel}$ and $D^{\perp}$ [50].

Following the idea of Archer and Evans [30] one can integrate the Smoluchowski equation by now applying $N\int \mathrm{d}^3r_2\cdots\int \mathrm{d}^3r_N\int \mathrm{d}^2u_1\cdots\int_{\mathrm{d}}^2 u_n$ on both sides of Eqn (1.100). This results in [49]:

$$\begin{aligned}\frac{\partial\rho(\vec{r},\hat{u},t)}{\partial t}=&\vec{\nabla}_{\vec{r}}\cdot\bar{\bar{D}}(\hat{u})\cdot\left[\vec{\nabla}_{\vec{r}}\rho(\vec{r},\hat{u},t)+\frac{1}{k_BT}\rho(\vec{r},\hat{u},t)\cdot\vec{\nabla}_{\vec{r}}V_{\mathrm{ext}}(\vec{r},\hat{u},t)-\frac{\vec{F}(\vec{r},\hat{u},t)}{k_BT}\right]\\&+D_r\hat{R}\cdot\left[\hat{R}\rho(\vec{r},\hat{u},t)+\frac{1}{k_BT}\rho(\vec{r},\hat{u},t)\vec{\nabla}_{\vec{r}}V_{\mathrm{ext}}(\vec{r},\hat{u},t)-\frac{1}{k_BT}\vec{T}(\vec{r},\hat{u},t)\right]\end{aligned} \tag{1.103}$$

with an average force

$$\vec{F}(\vec{r},\hat{u},t)=-\int \mathrm{d}^3r'\int \mathrm{d}^2u'\ \rho^{(2)}(\vec{r},\vec{r}',\hat{u},\hat{u}',t)\vec{\nabla}_{\vec{r}}v_2(\vec{r}-\vec{r}',\hat{u},\hat{u}') \tag{1.104}$$

and average torque

$$\vec{T}(\vec{r},\hat{u},t) = -\int \mathrm{d}^3r' \int \mathrm{d}^2u' \ \rho^{(2)}(\vec{r},\vec{r}',\hat{u},\hat{u}',t)\hat{R}v_2(\vec{r}-\vec{r}',\hat{u},\hat{u}') \quad (1.105)$$

The two-particle density which is in general unknown can be approximated in equilibrium by using

$$\vec{F}(\vec{r},\hat{u},t) = \rho_0(\vec{r},\hat{u})\vec{\nabla}_{\vec{r}}\frac{\delta\mathcal{F}_{\mathrm{exc}}(T,[\rho_0])}{\delta\rho_0(\vec{r},\hat{u})} \quad (1.106)$$

respectively

$$\vec{T}(\vec{r},\hat{u},t) = \rho_0(\vec{r},\hat{u})\hat{R}\frac{\delta\mathcal{F}_{\mathrm{exc}}[\rho]}{\delta\rho_0(\vec{r},\hat{u})} \quad (1.107)$$

Similar as in the isotropic (spherical) case we now employ the "adiabatic" approximation. We assume that the pair correlations in nonequilibrium are the same as those for an equilibrium system with the same one-body density profile (established by a suitable $V_{\mathrm{ext}}(\vec{r},\hat{u},t)$). The resulting dynamical equation for the time-dependent one particle density $\rho(\vec{r},\hat{u},t)$ is then given by Ref. [49]:

$$\begin{aligned} k_BT\frac{\partial\rho(\vec{r},\hat{u},t)}{\partial t} &= \vec{\nabla}_{\vec{r}}\cdot\bar{\bar{D}}(\hat{u})\cdot\left[\rho(\vec{r},\hat{u},t)\vec{\nabla}_{\vec{r}}\frac{\delta\mathcal{F}[\rho(\vec{r},\hat{u},t)]}{\delta\rho(\vec{r},\hat{u},t)}\right] \\ &\quad + D_r\hat{R}\left[\rho(\vec{r},\hat{u},t)\hat{R}\frac{\delta\mathcal{F}[\rho(\vec{r},\hat{u},t)]}{\delta\rho(\vec{r},\hat{u},t)}\right] \end{aligned} \quad (1.108)$$

with the equilibrium Helmholtz free energy density functional

$$\begin{aligned} \mathcal{F}[\rho] &= k_BT\int \mathrm{d}^3r \int \mathrm{d}\hat{u} \ \rho(\vec{r},\hat{u})\left[\ln(\Lambda^3\rho(\vec{r},\hat{u})) - 1\right] \\ &\quad + \mathcal{F}_{\mathrm{exc}}(T,[\rho]) + \int \mathrm{d}^3r \int \mathrm{d}\hat{u} \ \rho(\vec{r},\hat{u})V_{\mathrm{ext}}(\vec{r},\hat{u},t) \end{aligned} \quad (1.109)$$

This sets the frame for dynamical density functional theory (DDFT) for rods.

As for a special application of DDFT to dynamics in the confined isotropic phase we refer to [49] where the mean-field approximation for the functional was employed. More recent work has used the Rosenfeld functional for hard spherocylinders [48] for driven nematic phases [51, 52].

3.4. *"Active" (self-propelled) Brownian particles*

"Active" particles are self-propelled by their own intrinsic motor. In fact, apart from swimming bacteria, there are artificial microswimmers made by colloidal particles [53, 54]. Ignoring hydrodynamic interactions, these swimmers can simplest be modelled by rod-like particles which are driven by a constant force along their orientations; the force corresponds to an effective drift velocity and mimicks the actual propulsion mechanism. On top of the intrinsic propulsion, the particles feel Brownian noise of the solvent. The corresponding motion is intrinsically a nonequilibrium one and even the dynamics of a single Brownian swimmer was solved only recently [55, 56].

Starting from the Smoluchowski equation with an appropriate intrinsic drift term, a dynamical density functional theory can be derived using the same adiabatic approximation (1.64) as in the "passive" case. The resulting equation of motion for the one-particle density then [57] has an extra term on the right-hand side of Eqn. (1.108), namely

$$-F_0\vec{\nabla}\bar{\bar{D}}(\hat{u})\rho(\vec{r},\hat{u},t)\hat{u} \tag{1.110}$$

where F_0 denotes the internal driving force. This represents a microscopic theory for concentrated "active" matter. For swimmers in a two-dimensional channel, the time-dependent density profiles were found to be in agreement with Brownian dynamics computer simulations [57] even if a crude Onsager-like density functional approximation [43] was used. Qualitatively, the transient formation of hedgehog-like clusters ear the channel boundaries was reproduced by the dynamical density functional theory.

4. Conclusions

In conclusion, there is a variety of topologies for equilibrium phase diagrams, even for relatively simple radially-symmetric pair potentials $V(r)$. Examples include freezing into crystalline lattices with unusual open structure and reentrant melting effects if the interaction is soft and isostructural solid-to-solid transition for system with short-ranged attractions. The effects are predicted by Monte Carlo computer simulations and can in principle be confirmed by density functional theory of freezing. Colloidal particles can be used as model systems to realize these interactions.

Rod-like systems with anisotropic interactions, on the other hand, exhibit liquid crystalline phase with different degrees of orientational and

positional ordering. Again density functional theory of freezing can be formulated and be applied to predict the topology of the phase diagram. Rod-like colloidal particles represent ideal model systems to explore and test the phase behaviour experimentally.

Effects of colloidal dynamics in a solvent both in equilibrium and nonequilibrium are conveniently simulated by Brownian dynamics computer simulations. The density functional theory can be extended towards dynamics, so-called dynamical density functional theory to tackle various nonequilibrium phenomena. This was demonstrated for crystal growth at imposed nucleation seeds and for the collective behaviour of "active" Brownian particles. In general, dynamical density functional theory is in good agreement with the simulations. This may be different for undamped Newtonian dynamics which occurs for example in molecular liquid crystals or in a complex plasma [58].

Acknowledgement: I thank R. Evans, M. Rex, H. H. Wensink, S. van Teeffelen, U. Zimmermann, T. Glanz, M. Kohl and A. Härtel for many helpful suggestions. This work was supported by the DFG (SPP1296 and SFB TR6 (project D3)).

References

[1] A. F. Thünemann, M. Müller, H. Dautzenberg, J.-F. Joanny, H. Löwen, Adv. Polym. Sci. **166**, pages 113-171 (2004), Springer Series.
[2] H. Löwen, G. Kramposthuber, Europhys. Letters **23**, 637-678 (1993).
[3] G. A. Vliegenthart, P. van der Schoot, Europhys. Lett. **62**, 600-606 (2003).
[4] J. Dzubiella, H. Löwen, C. N. Likos, Phys. Rev. Letters **91**, 248301 (2003).
[5] M. Doi, S. F. Edwards, The Theory of Polymer Dynamics, Oxford Science Publications, Clarendon Press Oxford (1986).
[6] J. K. G. Dhont, An Introduction to Dynamics of Colloids, Elsevier, Amsterdam, 1996.
[7] H. Löwen, J. Phys.: Condensed Matter **13**, R415-R432 (2001).
[8] H. Löwen, Soft Matter, DOI:10.1039/b923685f, in press.
[9] R. Roth, J. Phys.: Condensed Matter **22**, 063102 (2010).
[10] R. Evans, Advances in Physics **28**, 143 (1979).
[11] D. W. Oxtoby, in: Liquids, Freezing and Glass Transition, edited by J. P. Hansen, D. Levesque, J. Zinn-Justin, North Holland, Amsterdam, pages 145-189, 1991.
[12] H. Löwen, Physics Reports **237**, 249 (1994).
[13] J.-L. Barrat, J.-P. Hansen, Basic Concepts for Simple and Complex Liquids, Cambridge University Press, 2003.

[14] H. Löwen, J. Phys.: Condensed Matter **14**, 11897 (2002).
[15] P. Tarazona, J. A. Cuesta, Y. Martinez-Raton, Density functional Theories of Hard Particle Systems, Lect. Notes Phys. **753**, Springer, Berlin, pages 247-341 (2008).
[16] J. P. Hansen, I. McDonald, Theory of Simple Liquids. 3rd Edition, Elsevier, Amsterdam, Academic Press 2005.
[17] M. P. Allen, D. J. Tildesley, Computer Simulation of Liquids, Oxford Science Publications, Clarendon Press, Oxford, 1987.
[18] C. N. Likos, Z. T. Németh, H. Löwen, J. Phys.: Condensed Matter **6**, 10965 (1994).
[19] C. N. Likos, H. Löwen, M. Watzlawek, B. Abbas, O. Jucknischke, J. Allgaier, D. Richter, Phys. Rev. Letters **80**, 4450 (1998).
[20] M. Watzlawek, C. N. Likos, H. Löwen, Phys. Rev. Letters. **82**, 5289 (1999).
[21] A. Lang, C. N. Likos, M. Watzlawek, H. Löwen, J. Phys.: Condensed Matter **12**, 5087 (2000).
[22] D. Gottwald, C. N. Likos, G. Kahl, H. Löwen, Phys. Rev. Letters **92**, 068301 (2004).
[23] C. N. Likos, A. Lang, M. Watzlawek, H. Löwen, Phys. Rev. E **63**, 031206 (2001).
[24] R. Ohnesorge, H. Löwen, H. Wagner, Europhys. Letters **22**, 245 (1993).
[25] A. J. Archer, Phys. Rev. E **72**, 051501 (2005).
[26] S. van Teeffelen, N. Hoffmann, C. N. Likos, H. Löwen, Europhysics Letters **75**, 583 (2006).
[27] Y. Rosenfeld, M. Schmidt, H. Löwen, P. Tarazona, Phys. Rev. E **55**, 4245 (1997).
[28] P. Tarazona. Phys. Rev. Letters **84**, 694 (2000).
[29] P. N. Pusey, in: Liquids, Freezing and Glass Transition, edited by J. P. Hansen, D. Levesque, J. Zinn-Justin, North Holland, Amsterdam, pages 145-189, 1991.
[30] A. J. Archer, R. Evans, J. Chem. Phys. **121**, 4246 (2004).
[31] U. M. B. Marconi, P. Tarazona, J. Chem. Phys. **110**, 8032 (1999).
[32] U. M. B. Marconi, P. Tarazona, J. Phys.: Condensed Matter **12**, A413 (2000).
[33] P. Español, H. Löwen, J. Chem. Phys. **131**, 244101 (2009).
[34] J. E. Hug, F. van Swol, C. F. Zukoski, Langmuir **11**, 111 (1995).
[35] R. J. Hunter, Foundations of Colloid Science. 2nd ed. Oxford University Press, Oxford, 1989.
[36] N. Hoffmann, F. Ebert, C. N. Likos, H. Löwen, G. Maret, Phys. Rev. Letters **97**, 078301 (2006).
[37] L. Assoud, F. Ebert, P. Keim, R. Messina, G. Maret, H. Löwen, Phys. Rev. Letters **102**, 238301 (2009).
[38] S. van Teeffelen, C. N. Likos, H. Löwen, Phys. Rev. Letters **100**, 108302 (2008).
[39] G. Kahl, H. Löwen, J. Phys.: Condensed Matter **21**, 464101 (2009).
[40] S. van Teeffelen, R. Backofen, H. Löwen, A. Voigt, Phys. Rev. E **79**, 051404 (2009).

[41] M. Rex, H. Löwen, Phys. Rev. Letters **101**, 148302 (2008).
[42] D. Frenkel, in: Liquids, Freezing and Glass Transition, edited by J. P. Hansen, D. Levesque, J. Zinn-Justin, North Holland, Amsterdam, pages 689-756, 1991.
[43] L. Onsager, Proc. New York Acad. Sci. **51**, 627 (1949).
[44] P. Bolhuis, D. Frenkel, J. Chem. Phys **106**, 666 (1997).
[45] D. Frenkel, B. M. Mulder, J. P. McTague, Phys. Rev. Letters **52**, 287 (1984).
[46] A. Poniewierski, R. Holyst, Phys. Rev. Letters **61**, 2461 (1988).
[47] H. Graf, H. Löwen, J. Phys.: Condensed Matter, **11**, 1435 (1999).
[48] H. Hansen-Goos, K. Mecke, Phys. Rev. Letters **102**, 018302 (2009).
[49] M. Rex, H. H. Wensink, H. Löwen, Phys. Rev. E **76**, 021403 (2007).
[50] H. Löwen, Phys. Rev. E **50**, 1232 (1994).
[51] A. Härtel, H. Löwen, J. Phys.: Condensed Matter **22**, 104112 (2010).
[52] A. Härtel, R. Blaak, H. Löwen, to be published.
[53] R. Dreyfus, J. Baudry, M. L. Roper, M. Fermigier, H. A. Stone, J. Bibette, Nature **437**, 862-865 (2005).
[54] A. Erbe, M. Zientara, L. Baraban, C. Kreidler, P. Leiderer, J. Phys.: Condensed Matter **20**, 404215 (2008).
[55] S. van Teeffelen, H. Löwen, Phys. Rev. E **78**, 020101 (2008).
[56] B. ten Hagen, S. van Teeffelen, H. Löwen, Condensed Matter Physics **12**, 725-738 (2009).
[57] H. H. Wensink, H. Löwen, Phys. Rev. E **78**, 031409 (2008).
[58] G. E. Morfill, A. V. Ivlev, Rev. Mod. Phys. **81**, 1353-1404 (2009).